Science of the Total Environment 1004 (2025) 180823

Contents lists available at ScienceDirect

Science of the Total Environment

journal homepage: www.elsevier.com/locate/scitotenv

Flow-interruption experiments to quantify trace elements leaching from a shallow saline aquitard

Abraham Ofori [a], Luigi Alessandrino [a], Regmi Vipin [b], Micòl Mastrocicco [a], Nicolò Colombani [b,*]

[a] DiSTABiF - Department of Environmental, Biological and Pharmaceutical Sciences and Technologies, Campania University "Luigi Vanvitelli", Via Vivaldi 43, 81100, Caserta, Italy
[b] SIMAU - Department of Materials, Environmental Sciences and Urban Planning, Marche Polytechnic University, Via Brecce Bianche 12, 60131, Ancona, Italy

HIGHLIGHTS

- Flow interruption in columns assessed TE mobility in salinized peaty aquitard
- Sequential extraction quantified the limited extent of pyrite oxidation
- Flow interruptions showed peaks of As, Mn, Pb and Ni exceeding WHO standards
- Irrigation periods after prolonged drought could trigger TE mobility

GRAPHICAL ABSTRACT

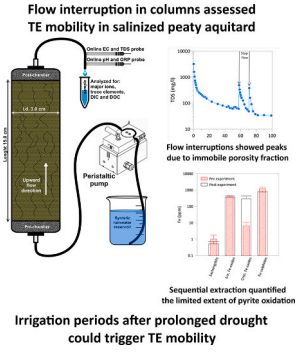

ARTICLE INFO

Keywords:
Column leaching experiments
Pyrite oxidation
Trace elements mobility
Sequential extraction
Groundwater freshening

ABSTRACT

Salinity from reclaimed lands in coastal deltaic areas is of upcoming concern throughout the world due to the ongoing climatic change and the associated water resources overexploitation. Sub-irrigation in salinized deltaic soils can promote the transport of major and trace elements (TE) in groundwater. In this study, experiments on flow interruption in columns have been conducted for salinized peaty aquitard from the Po Delta using synthetic rainwater to replicate sub-irrigation practices and their effect on TE leaching. Non-equilibrium transport and cation exchange phenomena were assessed using a NaCl tracer test. This latter was also simulated via CXTFIT 2.0 to quantify sorption and physical non-equilibrium processes. Pre and post experiment sequential extraction allowed for the evaluation of geochemical alterations caused by the injection of the synthetic rainwater and the tracer solution into the reducing sediments. Results from the flow interruptions showed peaks of As, Mn, Pb, and Ni exceeding the World Health Organization standards for drinking water, indicating that irrigation periods are marked by the diffusion of trace elements hosted in exchange sites and solid phases. The employment of NaCl as a tracer resulted in a significant elution of trace elements due to Na^+ exchange from clays and organic matter and retardation of Cl^- due to diffusion into the osmotic membranes of organic fragments. The partial oxidation of pyrite and arsenopyrite to Fe(III) oxides contributes to the prolonged release of TE. These results highlight how alternating sub-irrigation in a peaty reducing environment can trigger the mobilization of TE in deltaic contexts.

* Corresponding author.
E-mail address: n.colombani@univpm.it (N. Colombani).

https://doi.org/10.1016/j.scitotenv.2025.180823
Received 4 July 2025; Received in revised form 26 September 2025; Accepted 25 October 2025

The findings of this study are of relevance, as similar hydrogeological settings are widespread globally. Indeed, in real-world scenarios, such as agricultural systems with intermittent irrigation or aquifer restoration strategies, flow interruptions are commonly utilized worldwide.

1. Introduction

In the modern Delta plains, it is known that saline conditions may mobilize the trace elements (TE) naturally present in the soils and sediments (Du Laing et al., 2009; Gantayat and Elumalai, 2024) or anthropogenically introduced (Gu et al., 2013; Qian et al., 2015). Many are the examples around the world where this process is reported to occur: the Pearl River Delta (Wang et al., 2016) and the Yellow River Delta (Li et al., 2020) in China, the Sacramento–San Joaquin Delta in California, USA (Pasternack and Brown, 2006), the Bengal Delta in India (Farooq et al., 2010), the Nile Delta in Egypt (Said et al., 2022), and the Po River Delta in Italy (Di Giuseppe et al., 2014; Giambastiani et al., 2024). TE mobility in soils and waters (surface and groundwater) is controlled by ionic strength, surface complexation, oxidation-reduction, and precipitation-dissolution reactions (Caporale and Violante, 2016), and their presence among sediments comprises: water-soluble, exchangeable, carbonate-bound, reducible, oxidizable, and residual fractions (Sarkar et al., 2014). Redox potential, temperature, pH, and concentrations of organic ligands are some environmental variables that can change and release TE from the solid to the liquid phase, eventually contaminating nearby surface waters and groundwater (Sahuquillo et al., 2003). Soil water fluctuations are often the driver of redox and pH shifts, inducing sedimentary organic matter (SOM) mineralization and pedogenic oxides precipitation/dissolution (Schulz-Zunkel and Krueger, 2009), which in turn can immobilize or mobilize TE (Pelfrêne et al., 2009). Nevertheless, only few studies have tackled the influence of soil water fluctuations on TE mobility in synthetic numerical experiments (Jacques et al., 2008) or field-based experiments (Li et al., 2022a, 2022b).

Some TE, like most of heavy metals or Arsenic (As), are recognized as carcinogenic and toxic. A particular concern arises when elevated TE concentrations are detected in ground and surface water due to natural background levels and anthropogenic activities such as mining (Rahman and Singh, 2019; Shams et al., 2022). For instance, As is naturally sourced from the oxidation of sulphide minerals, particularly arsenopyrite (FeAsS) (Corkhill and Vaughan, 2009), or even arsenian pyrite that typically contains up to 10.0 wt% of As, since it can randomly substitute for S in the crystalline lattice (Blanchard et al., 2007). Generally, an increase in pH along with the presence of Fe^{3+}, bacteria, or both, results in enhanced oxidation rates of As-bearing sulphides; except for FeAsS, whose oxidation by dissolved oxygen (DO) is pH independent and accelerates with rising DO levels (Lengke et al., 2009). The oxidation rate of pyrite is observed to be complexly dependent on the surface area and extent of the reaction (Appelo et al., 1998). Pyrite oxidation in sediments can be represented by the following stoichiometric reaction:

$$FeS_{2(s)} + \frac{15}{4}O_{2(g)} + \frac{7}{2}H_2O_{(aq)} \rightarrow Fe(OH)_{3(s)} + 2SO^{2-}_{4(aq)} + 4H^{+}_{(aq)} \quad (1)$$

and it may exhibit spatial heterogeneity, potentially driven by local pH fluctuations (McKibben and Barnes, 1986). Additionally, as the reaction progresses, the Fe-oxide layers may inhibit the oxidation rate (Wang et al., 2019). For instance, the oxidation of framboidal pyrite leads to a drop in pH, resulting in the release of an acidic solution, then As is simultaneously released as an impurity of framboidal pyrite (Chandra and Gerson, 2010), with redox reactions reportedly being the main driver for the release of As, Cd, Ni, Cu, Zn, and Mn from rock, sediment, and soil (Frohne et al., 2011).

The subsurface transport of TE is governed by a suite of geochemical processes such as adsorption, desorption, precipitation, and complexation with coexisting ions. Low ionic strength of the leaching water tends to hinder the mobility of dissolved TE by enhancing competitive adsorption and complexation, whereas high ionic strength conditions facilitate TE transport, primarily in colloid-bound forms (Wikiniyadhanee et al., 2015). As a result, flow experiments involving TE are typically characterized by nonequilibrium conditions (Tran et al., 1998). A simple and robust method for probing nonequilibrium processes during a flow experiment is the flow interruption method (Wehrer and Totsche, 2008). The flow interruption in column experiments aims to provide the solute with sufficient time to be adsorbed on the sorption sites and characterized as a diffusion-dominated process (Tran et al., 1998). Whether the flow is interrupted during an arrival, or an elution breakthrough determines if the concentrations following a stop flow will increase or decrease when flow is restarted (Wehrer and Totsche, 2008). TE mobility can be changed by microbial and plant growth through pH and Eh alteration (Husson, 2013). Under oxidizing conditions, TE mobility is limited since they often co-precipitate within metal oxides or are adsorbed/complexed on metal oxides or clay surfaces (Bao et al., 2022). Pristine peatlands serve as sinks for atmospheric carbon due to the slowed decomposition caused by a prolonged absence of oxygen (Freeman et al., 2001), as reducing conditions result in decreasing dissolved organic carbon (DOC) (Höll et al., 2009), making peaty soils the largest pool of terrestrial organic carbon (Gorham, 1991). Therefore, in soils and sediments rich in sedimentary organic matter (SOM), reducing conditions commonly prevail, promoting the dissolution of Fe and Mn-(hydr)oxides, mobilizing also the co-precipitated and adsorbed TE (Li et al., 2022a, 2022b). Conversely, when SOM degradation progresses and sulphate reduction is the dominating electron accepting process, TE immobilization is again induced by the precipitation of TE sulphides (Vink et al., 2010). Besides, TE can be mobilized by saltwater (Bäckström et al., 2004) as ionic strength variations affect TE mobility in sediments and subsequently their bioavailability (Li et al., 2016), as well as DOC due to aqueous complexes formation (Pérez-Esteban et al., 2013; Seuntjens et al., 2004). Interestingly, salinity induced by NaCl and other Cl^- salts ignites high TE release from soils (Acosta et al., 2011). In this pursuit, NaCl as a tracer in flow experiments has been widely employed in literature since Cl^- acts as a natural tracer due to its resistance to microbial degradation and its negligible tendency to form ionic complexes (Botter et al., 2008; Mastrocicco et al., 2011; Tran et al., 1998). In addition to aqueous complexation, the cation exchange capacity (CEC) of soils and sediments is also implicated in TE mobilization/immobilization via exchange sites present in both clays and SOM (Fontes and dos Santos, 2010). Indeed, Na^+ may be exchanged with other cations such as Ca^{2+} and Mg^{2+}, as commonly reported in aquifers with clay minerals (Capuano and Jones, 2020; Eeman et al., 2017) and may mobilize other TE on the mineral surface into solution due to cation exchanges (Mora et al., 2020).

One dimensional numerical and analytical models are widely used for solute transport in porous media (Feinstein and Guo, 2004; Mastrocicco et al., 2011; Saaltink and Rodríguez-Escales, 2022). CXTFIT 2.1, included in the graphical user interface STANMOD, is one of the most robust analytical codes supporting deterministic runs of one-dimensional advection-dispersion equations and associated inverse models (Toride et al., 1995). It solves the inverse problem by optimizing the fit between computed and observed concentrations at specified locations and times (Feinstein and Guo, 2004). CXTFIT 2.1 is widely employed in column experiments in the analysis of solute transport in groundwater and porous media to delineate salinization, contaminants flow, and redox processes in nature (Kiecak et al., 2019; Tiemeyer et al., 2017). Thus, this study aimed i) to quantify the leaching behaviour of major ions and TE in a silty-clay aquitard rich in SOM subjected to sub-

irrigation, ii) to evaluate the influence of flow interruptions coupled with saltwater input on the cumulative leaching of selected TE, and iii) to quantify the solute transport behaviour of these shallow saline aquitard sediments using different modelling approaches. To this end, column experiments were performed and modelled in saturated conditions, and chemical sequential extraction from the solid phases was employed to quantify the relative pools mobility of selected TE.

2. Materials and methods

2.1. Site information and soil sampling

Sediment sampling was conducted in an agricultural field in the Po lowland (Northern Italy) near Berra village, 24 km from the Adriatic Sea (44°56′52.37″N and 12°01′37.44″E) at an elevation of approximately −3 m above sea level (asl). Indeed, the area has been completely reclaimed at the end of 19th century and is now drained by an extensive system of canals and reclamation ditches, managed by pumping stations that regulate the shallow groundwater table (Gaiolini et al., 2025). This site was chosen because it is representative of the geomorphological characteristics of the Po delta lowland and of the anthropo-geological evolution of the region, which is nearly totally below sea level due to the massive land reclamation efforts for agricultural purposes (Simeoni and Corbau, 2009). Tile drains, with a diameter of 5 cm, made of steel and spaced 10 m apart, have been installed, with depths ranging from 0.90 m near the ditches to 0.70 m below ground level at the end of the field. This system has been operational since 2018 to prevent waterlogging and to remove excess saline water, as the area is characterized by paleo salinity trapped in pore spaces of low permeability lenses and SOM (Habakaramo Macumu et al., 2024). The tile drains facilitate sub-irrigation when the inlet valve from the main irrigation channel is opened, and weirs are positioned at the ends of the nearby ditches.

Duplicate soil samples were collected in two locations named Column 1 and Column 2, placed 3 m apart from each other. Soil samples exuded with an Eijkelkamp auger corer for minimum disturbance of soft soils, between the depths of 0.75 to 1.00 m below ground level where the water table usually fluctuates due to tile drains location, and were kept in a vacuum sealed plastic bag and refrigerated at 4 °C. SOM was measured gravimetrically after combustion at 350 °C for 24 h (Table 1), the pH (1:5 in water) was measured from a sub sample aliquot of 10 g in each column. The CEC was determined by ammonium acetate extraction (pH 7.0), while carbonate content was measured titrimetrically after digestion with excess acid (HCl 1 N). The soil particle-size distribution was determined by the pipette method. The saturated hydraulic conductivity (k_{sat}) was measured via a constant head test at the end of the leaching experiment in each column.

2.2. Saturated column experiments design and set up

For the saturated leaching experiments, HDPE columns were used. Columns' dimensions were 15.0 cm in length and 3.0 cm in internal diameter (Fig. 1). To simulate the layering found in alluvial environments, the column was filled in 1–2 cm increments in a N_2 atmosphere within a glove bag to prevent redox alteration of the soil, each packed using a Teflon piston; while soil was not sterilized to minimize the alteration of its characteristics (Alessandrino et al., 2023; Lewis and Sjöstrom, 2010).

Columns were flushed via a peristaltic pump for at least 100 pore volumes to eliminate possible unwanted contaminants before each experiment was performed. At the top and bottom of the columns, high density polyethylene (HDPE) chambers were installed to uniform the flux and to prevent washing of finer grains. The chambers contained a HDPE pierced disc and a 50 μm NITEX mesh in contact with the soil. The flow direction was upward to eliminate the eventual formation of trapped gas bubbles. The porewater flow rate was set at 100 ml/h and was produced by a peristaltic pump (Gilson MINIPLUS 3) connected to the bottom of the column. Samples were taken using 10 ml PE vials at constant time intervals and filtered with a 0.45 μm polypropylene filter. Pore volumes of water in the column were defined as the volume of the column (excluding the inflow and outflow chambers) multiplied by the soil porosity, and more in detail, V_0 is the volume of water required to reach a pore volume, while V is the volume of water injected at a given time. Effluents were drained from the columns via a 2 mm internal diameter tube through a flow cell equipped with temperature, EC, TDS, pH, and ORP probes for continuous monitoring with a portable high-resolution professional multiparametric probe (HANNA 50110742 XS PC 7 Vio Multiparameter Portable Meter). The probes were calibrated using standard solutions at the beginning of each experiment. In column 1, two flow interruptions were made: the first flow interruption for this

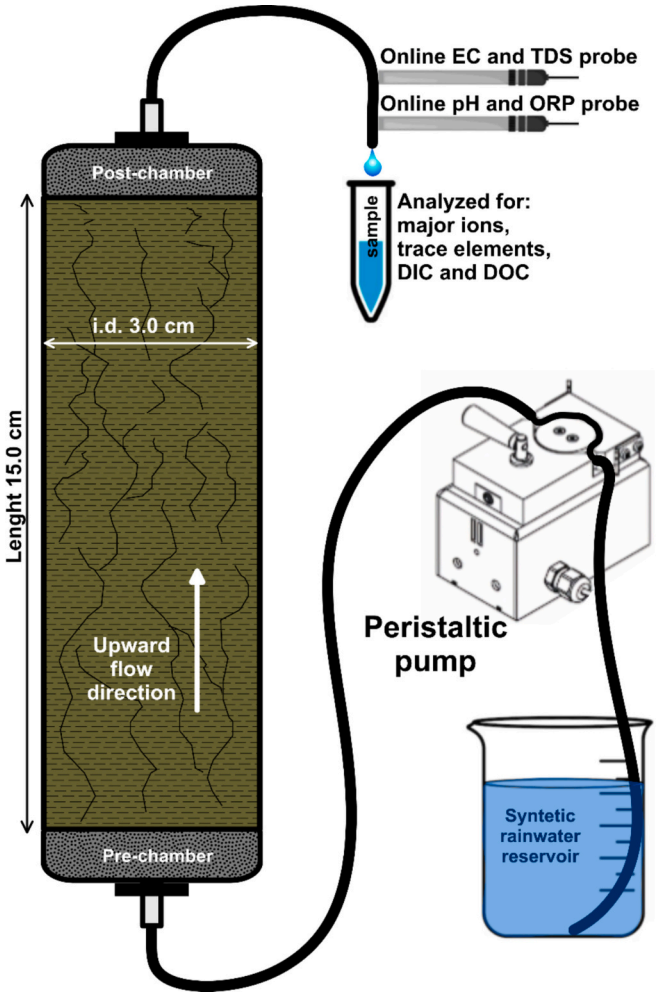

Fig. 1. Experimental set up of the upward saturated column apparatus.

Table 1
Soil physical-chemical characterization.

Sample	SOM (%)	pH (−)	CEC (meq/100 g)	Carbonates (%)	Clay (%)	Silt (%)	Sand (%)	K_{sat} (m/s)
Column 1	15.4	5.5	53.3	0.12	23.4	50.8	25.8	$7.3e^{-6}$
Column 2	25.6	5.4	61.8	0.15	25.1	48.9	26.0	$3.7e^{-6}$

experiment was made for 14 h, whereas the second flow interruption was made for 115 h, to enable sufficient solute diffusion (Tran et al., 1998). The design of the two distinct stop flow was chosen following the methods described by Kim and Hyun (2015). In addition, two different time intervals for the flow interruptions were chosen to capture both short-term and extended stagnation effects on solute mobilization. Indeed, different contact times can influence the leaching behaviour of certain solutes (López Meza et al., 2010) and using dual time scales has proven valuable outcomes from column leaching experiments as described by Tang et al. (2020). In column 2, a single flow interruption of 115 h was done. In column 2, 10 ml of NaCl with an EC of 11.4 mS/cm was used as a tracer, the flow was made to run with the synthetic rainwater after the NaCl dosage for 4 h until the effluent EC was constantly <100 μS/cm, with sampling made at 15 min intervals.

The cumulative mass of each dissolved species was calculated via temporal moment analysis, calculating the zero-order moment (Vincent et al., 2007).

2.3. Solute transport model

To quantify the dispersive solute transport in the packed columns, the transport behaviour of a conservative tracer (Cl^-) was simulated using the graphical user interface STANMOD (Van Genuchten et al., 2012) that is including CXTFIT 2.1, a one-dimensional solute transport model. The transport behaviour of solutes was described using the dual domain (DD) form of the advection dispersion equation (ADE) with linear retardation and constant production term (Eqs. (2)–(4)):

$$(\theta_m + \rho_b K_d)\frac{\partial C_m}{\partial t} = \theta_m D_m \frac{\partial^2 C_m}{\partial x^2} - J_w \frac{\partial C_m}{\partial x} - \alpha(C_m - C_{im}) + \theta_m \gamma_l(x) + \rho_b \gamma_s(x) \quad (2)$$

$$\theta_{im}\frac{\partial C_{im}}{\partial t} = \alpha(C_m - C_{im}) \quad (3)$$

$$R = 1 + \frac{K_d \rho_b}{\theta} \quad (4)$$

where subscripts $_m$ and $_{im}$ pertain to the mobile (liquid phase) and immobile (stagnant zones) region, respectively. C (ML^{-3}) denotes solute concentrations as a function of distance x (L) and time t (T). D_m (L^2T^{-1}) is the hydrodynamic dispersion coefficient for the mobile region, J_w (LT^{-1}) the volumetric water flux density, and the volumes θ (L^3L^{-3}), θ_m, (L^3L^{-3}), and θ_{im} (L^3L^{-3}) are the total, mobile and immobile water content. γ_m ($ML^{-3}\ T^{-1}$) and γ_s ($ML^{-3}\ T^{-1}$) are the zero order production terms for the liquid and sorbed phases, respectively. For $\theta_m = \theta$, Eq. (2) reduces to the single-domain ADE. The solute-mass transfer between mobile and immobile regions is limited by the first-order rate coefficient α (T^{-1}). R is the linear retardation factor, ρ_b (ML^{-3}) is the dry bulk density, and K_d (L^3M^{-1}) is the solid liquid distribution coefficient. The ADE was solved by the code CXTFIT 2.1 in estimation mode to fit observed Cl^- concentrations. The inverse problem is solved in CXTFIT 2.1 by minimizing an objective function that consists of the sum of the squared differences between observed and fitted concentrations. The objective function is minimized using a nonlinear least-squares inversion method to constrain the estimates of the upper and lower parameter values. The inverse model output provides useful model performance parameters like the coefficient of determination (R^2) from the regression of observed and calculated values, as well as the mean standard error (MSE) coefficient among observed and calculated values.

2.4. Analytical methods

Anions and cations were analysed with an ICS-1000 Dionex-Thermo Scientific chromatography system equipped with an isocratic dual pump. An IonPac AS14A 4 × 250 mm column and pre-column AG14A 4 × 50mm, and an ASRS-Ultra 4-mm self-suppressor were used for anions, while an IonPac CS12A 4 × 250 mm column and pre-column CS12A 4 × 50 mm CRS-500 4 mm self-suppressor were used for cations. The AS-40 Dionex auto-sampler was employed to run the analysis, while quality control (QC) samples were run every 10 samples. Detection limits were 50 μg/l for Ca^{2+} and Mg^{2+}, and 10 μg/l for the other ions. DOC was analysed with a Pharmacia Biotech Ultrospec 2000 UV/VIS spectrophotometer following the procedure of Cook et al. (2017), with a detection limit of 100 μg/l. DIC was determined titrimetrically (Huang et al., 2012; Dickson, 1981), with a detection limit of 100 μg/l. TE (Al, Li, Sr, Co, Cd, Cu, Mn, Mo, Ni, Be, Cr, Fe, Se, Si, V, and Zn) were analysed with an ICP-OES (PerkinElmer, USA) to quantify their concentration in water samples after acidification with ultrapure 1 M nitric acid, preceded by filtering on 0.45 μm. As was quantified also in ICP-OES, but in a second subsample with a hydride generator to avoid interference with other elements. All the equipment was correctly acid washed, and method blanks were carried out. Indeed, to successfully determine TE, such as As, Se, and Te, with the ICP-OES, hydride generation is required due to their low detection (Wiltsche et al., 2008; Wickstrøm et al., 1995). The addition of a reducing agent, such as sodium borohydride, converts these elements (As, Se, and Te) into their volatile hydrides, thereby boosting their sensitivities and lower detection limits below the low-μg/l range for easy detection by the ICP-OES (Yousefi and Zolfonoun, 2020). Nonetheless, hydride generation of these elements (As, Se, and Te) is subjected to interferences from other elements, such as Ni, Co, Cu, and Fe, and therefore requires a separate analysis, masking the interferents to minimize their effects, or fast separation of the hydride from the liquid phase, preceded by a rapid hydride generation (Ding and Sturgeon, 1997; Thangavel et al., 2015; Wickstrøm et al., 1995). Similarly, as 'labile' DOC affects the immobilization of TE and their biochemical cycles (Chakraborty and Chakrabarti, 2006), so is its quantification in water (surface and groundwater) analysis, as a filtration via 0.45 μm is adequate for its analysis by ISO 20236 protocols (Tisserand et al., 2024).

However, the ICP-OES is a versatile, effective, powerful, and advanced analytical technique with excellent detection properties in parts per million (ppm) and parts per billion (ppb) levels (Douvris et al., 2023) widely used for the analysis of various chemical elements, involving environmental monitoring, food analysis, and medical diagnostics (Khan et al., 2022). With remarkable success, the ICP-OES has been employed in the precise detection of TE in edible oils (Bakircioglu et al., 2013), plant extracts (D'Archivio et al., 2019), soil extracts (Kelepertzis and Stathopoulou, 2013; Nenova et al., 2018), and Rare Earth Elements in geological samples (Pradhan and Ambade, 2020). Finally, in water (surface and groundwater) analysis with the ICP-OES, samples are filtered with 0.45 μm membrane filters to remove particulates and colloids that would potentially clog nebulizers and skew the "dissolved" definition; followed by acidification with nitric acid (typically 1 % v/v HNO_3) to keep the pH <2, keeping metal ions in true solution, preventing precipitation and adsorption onto container walls (Khan et al., 2022; Standard Committee of Analysts, 2018; US EPA, 1996).

2.5. Sequential extraction from sediments

Three replicates for each sample employed for the column experiments were collected at the beginning and at the end of the experiment to perform the sequential extraction. The sediment of both columns was homogenized and subsequently re-divided in an inert environment into sub-aliquots. Each sub-aliquot was placed in a 50 ml polycarbonate centrifuge vial. Sequential extractions of TE adsorbed or co-precipitated in different pools of the sediments were performed using published methods (Sbarbati et al., 2020) in the sequence highlighted in Table 2. Individual aliquots of sediment (4 g dry weight) were treated sequentially with each extracting solution (solid:solution = 0.01 by mass), the suspensions centrifuged (25 min at 8500 rpm), and the supernatant decanted and filtered (0.45 μm nylon membrane filters). Between each extraction step, the sediments were washed with 40 ml of deionized

Table 2
TE sequential extraction procedure modified from Sbarbati et al. (2020).

Step	Extractant and time	Target Fe phase	Target TE
1	1 mol/l $MgCl_2$, pH 7, 2 h, one repetition	Exchangeable TE	Loosely bound TE
2	1 mol/l $NH_2OH{\cdot}HCl$ in 25 % v/v CH_3COOH, 48 h, one repetition	Amorphous Fe (III) oxides	TE in amorphous Fe-oxides
3	50 g/l $Na_2S_2O_4$, pH 4.8 with $CH_3COOH/C_6H_5Na_3O_7{\cdot}2H_2O$, 2 h, one repetition	Crystalline Fe (III) oxides	TE in crystalline Fe-oxides
4	16 mol/l HNO_3, 2 h, one repetition	Fe(II) sulphides	TE-bearing sulphides

water (18.2 MΩ), centrifuged, and the supernatant decanted. To successfully quantify TE in sediments, sequential extraction procedures were chosen since they are mostly employed as proposed by the European Community Bureau of Reference (BCR) (Davidson et al., 1994; de Andrade Passos et al., 2010; Kryc et al., 2003). Sequential extraction approaches facilitate the partitioning of trace elements into operationally defined categories such as the exchangeable, the carbonate-bound, the reducible (Fe-Mn oxides), the oxidizable (organic/sulphide), and the residual, hence improving their accurate quantification in soils. (Salomons and Förstner, 1980; Tessier et al., 1979). The outcomes of sequential extractions facilitate the forecasting of a specific TE's release by identifying the predominant fraction influenced by soil pH, redox potential, or organic matter changes as a result of flooding, drying, and acidification (Carrillo-González et al., 2006; Mensah and Amoakwah, 2024; Rao et al., 2008; Tessier et al., 1979). Thus, quantifying these "labile" pools of TE refines risk assessments far better than total metal concentration alone, determining whether a contaminated site poses a threat to the environment and thereby informing management strategies and remediation approaches (Bacon and Davidson, 2008; Tack and Verloo, 1995). Significantly, sequential extraction data facilitate the tracking of the transformation routes of sulphate oxidation in releasing As or immobilizing Pb and Zn by iron oxides (Gómez-Ariza et al., 1999; Keon et al., 2001).

3. Results

3.1. Saturated columns leaching experiments

In both experiments (Figs. 2 and 3), due to the preferential flow in macropores, Cl^- dropped rapidly during the elution, and then progressively increased because of the micropores' contribution (Colombani et al., 2020), combined with the diffusion from osmotic membranes constituted by the halophytic plants' residues present in the SOM (Habakaramo Macumu et al., 2024). In column 1, after approximately 18 porewater of flushing, an increase of Si and Fe was detected, most likely due to the acid-promoted weathering of Fe-silicate phases in an oxidative environment (Santelli et al., 2001). Column 2 exhibited an overall higher concentration of TE in the leachate, likely due to a greater abundance of SOM (Table 1), which can act as an additional source of TE (Habakaramo Macumu et al., 2024). The potential presence of higher amounts of pyrite may have further contributed to the release of these elements under oxidative conditions. Indeed, after approximately 40 pore volumes of continuous flushing with synthetic rainwater, a marked drop in pH accompanied by an increase in ORP, SO_4^{2-}, DIC, and Ca^{2+} was observed, indicating the oxidation of more crystalline pyrite or coated by passivation layers (Fan et al., 2022). In both column experiments, As concentrations exhibited a notable decline, dropping well below the WHO threshold after approximately 18 pore volumes, followed by a subsequent increase between 30 and 40 pore volumes. The pH drops due to pyrite oxidation, triggered a slight increase in Mn and Al concentration in the leaching water since these two species are known to have a pH-dependent solubility (Sposito, 1995). However, Mn concentrations dropped below the provisional WHO limit (0.08 mg/l) in both experiments after approximately 35–40 pore volumes. The sediments of the Po River are naturally enriched in Ni due to the weathering of Ophiolite rocks, while Pb is relatively low (Bianchini et al., 2012). Consequently, in these experiments, the initial Ni concentration was an order of magnitude greater than that of Pb. Despite this, Ni concentration in the leachate was exceeding the WHO threshold (0.07 mg/l) only in the first step of the experiments, decreasing below the limit after approximately 10 pore volumes in both columns. However, Pb concentration in the leachate sample from column 2 initially exceeded the WHO threshold (0.01 mg/l), whereas in column 1, Pb concentrations were very close to this threshold, again indicating elevated heterogeneity of TE distribution within these aquitards. After approximately 20–25 pore volumes, Pb concentration decreased significantly below the WHO limit and remained consistently low for the remainder of the experiments. Overall, exceedances of the WHO limits were observed for most TE during the initial phase of both columns, indicating that continuous irrigation can leach these TE that may end up in the groundwater and surface water through the tile drainage systems and might negatively affect environmental conditions (Dahmouni et al., 2018). After approximately 20 pore volumes, all the analysed species decreased to concentrations below their respective WHO thresholds, meaning that many cycles of sub-irrigation are needed to completely flush TE. Each stop flow event triggered a renewed increase in concentration, leading to the exceedance of the WHO limits for As, Mn, Pb, and Ni.

3.2. NaCl tracer test

The tracer test was conducted on column 2 at the end of the leaching experiment. Prior to the test, the column was flushed again with synthetic rainwater for approximately 100 pore volumes, until the EC of the effluent stabilized <100 μS/cm and the concentrations of TE fell below their respective detection limits. NaCl solution was used to mimic the effect of brackish groundwater upward flow that could be further evapoconcentrated in soils. Indeed, in coastal areas, salt can be present in groundwater or be delivered through wet and dry deposition of sea spray and salinized irrigation water and then can be evapoconcentrated by plant roots (Ma et al., 2023). As showed in Fig. 4, even the low ionic strength associated with the NaCl tracer solution mobilized several major and TE. It must be stressed that As and Pb concentrations, with peaks of 0.022 mg/l and 0.034 mg/l respectively, exceeded the WHO threshold limits, although no TE were detected during the previous flushing.

3.2.1. CXTFIT results using different modelling approaches

Among the tested models, the Cl^- breakthrough curve obtained with DD + R + γ provided the best agreement with experimental data, outperforming both DD and ADE models (Fig. 5). This is also pointed out by the elevated R^2 obtained for DD + R + γ (Table 3). The ADE model, the most basic among those tested, accounts solely for solute transport via advection and dispersion, assuming negligible solute-soil interactions. The failure of the ADE approach is not a surprise, because a percentage of the overall porosity was found to be immobile (Table 3), as it can be expected for silty clay sediments (Mastrocicco et al., 2011; Zhang et al., 2022). On the other hand, the DD model incorporates the dual-porosity behaviour, which allows for partially reproducing the tailing observed in the Cl^- breakthrough curve. However, it still falls short of accurately capturing the full range of physical-chemical interactions with the soil matrix, particularly because it did not account for the potential contribution of SOM acting as an additional source of Cl^-. DD + R + γ model included the effects of dual-porosity, equilibrium retention processes, and kinetic sorption/desorption, which enables a more realistic representation of the transport mechanisms occurring within the system and the gradual release of additional Cl^- from the plant-derived SOM. Indeed, the estimated values of zero-production terms γ_l and γ_s provide valuable insights into the differential role of the two phases (liquid and

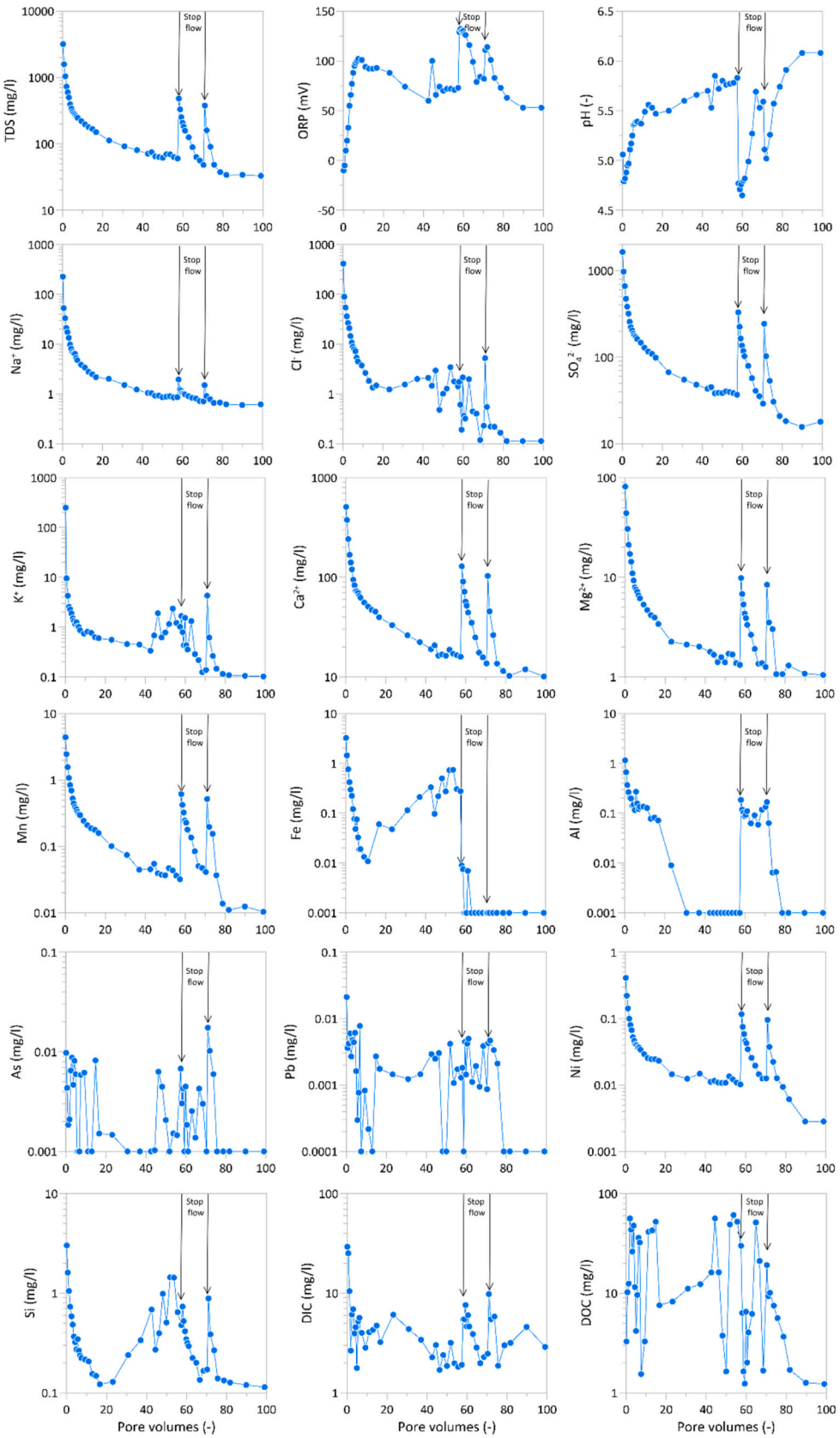

Fig. 2. Selected solute species of column experiment 1 with flow interruptions.

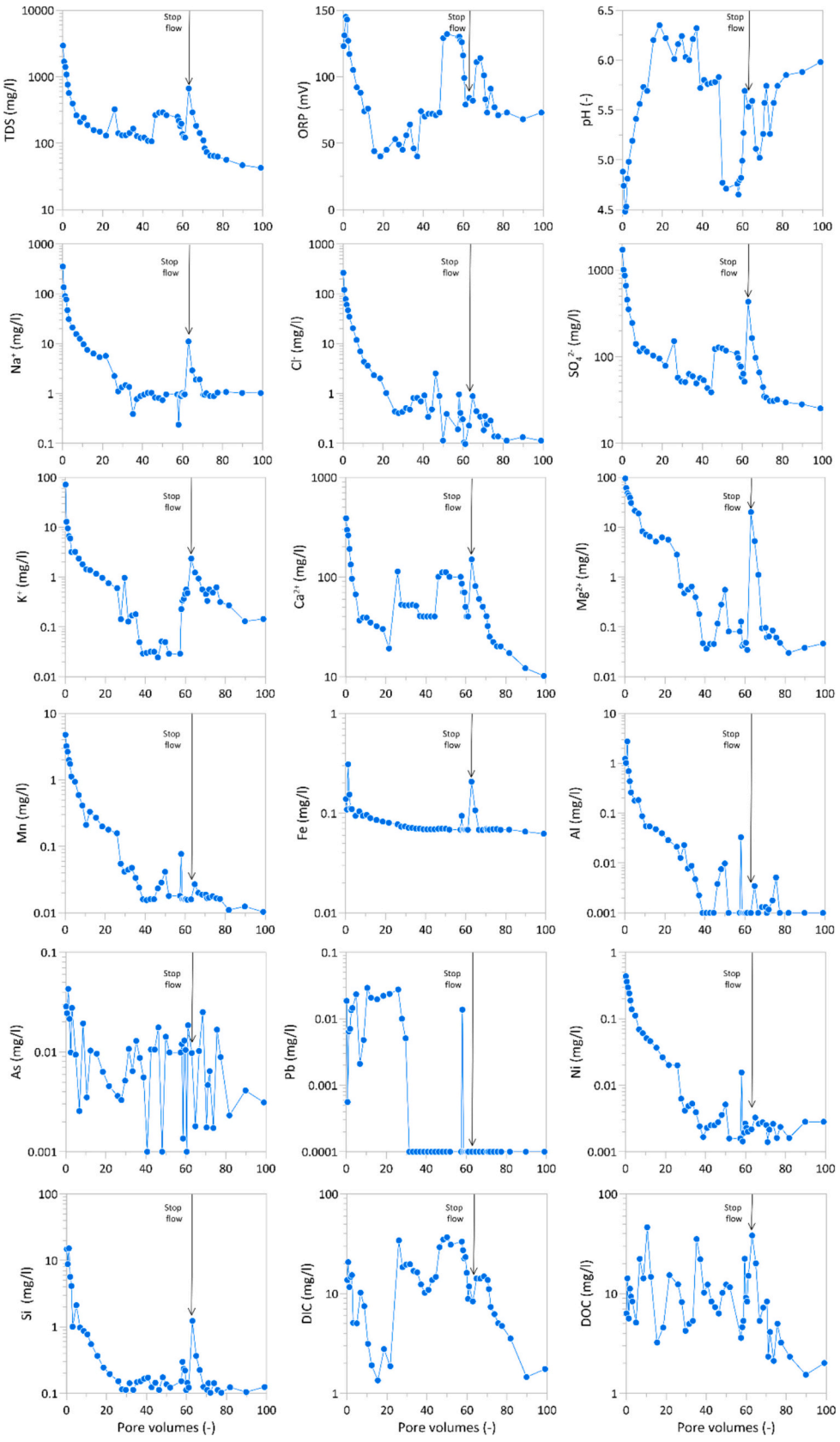

Fig. 3. Selected solute species of column 2 with flow interruption.

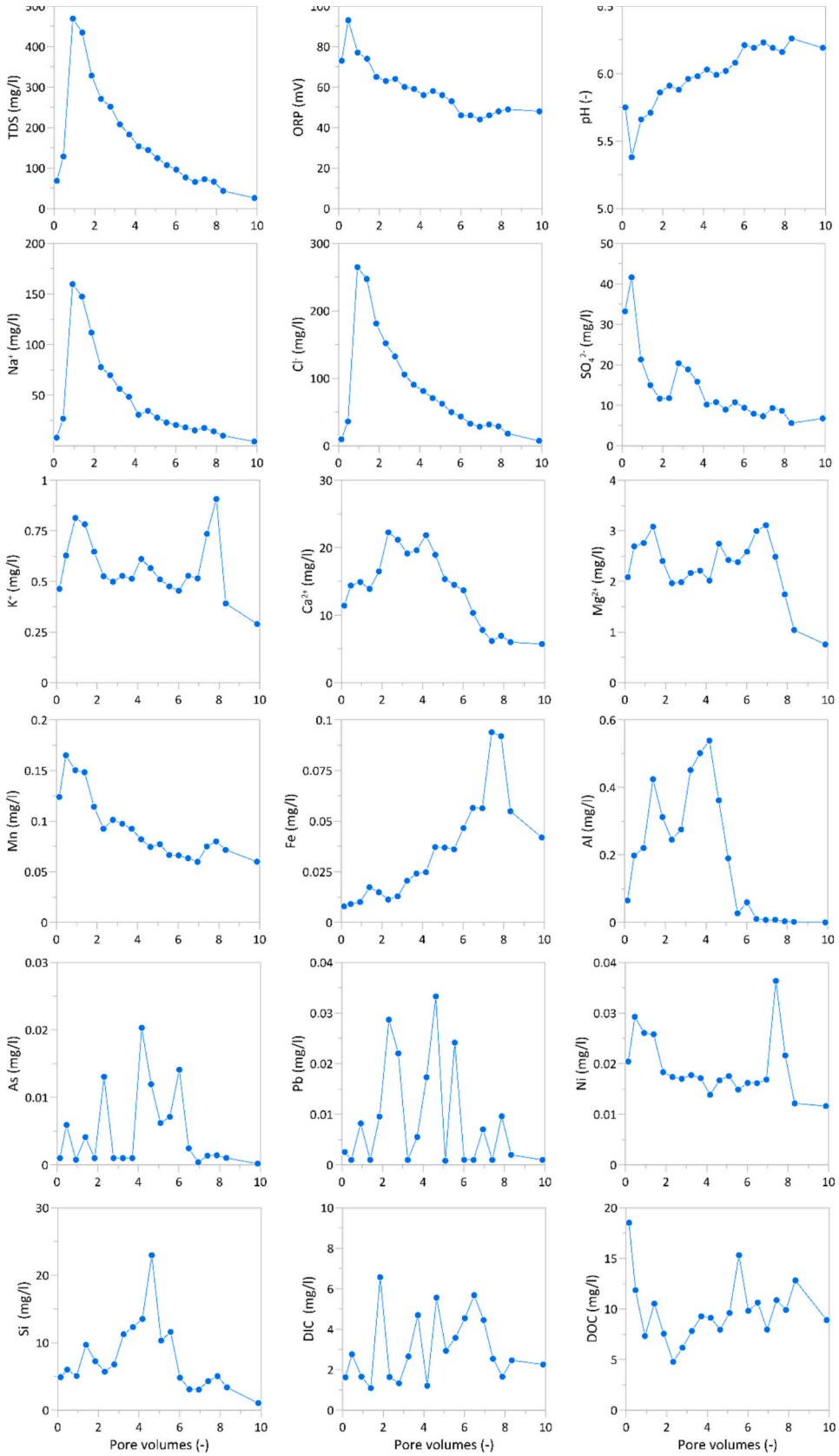

Fig. 4. TDS, ORP, pH and selected solute species of the NaCl tracer test in column 2.

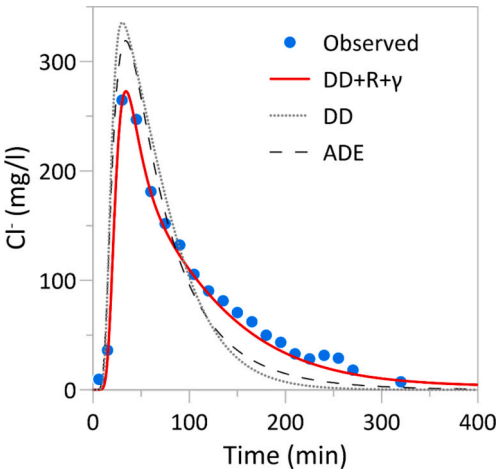

Fig. 5. Modelled Cl^- breakthrough curves with standard ADE, DD, and DD + R + γ.

Table 3
Performance indicators (R^2 and MSE) and parameters for the ADE, DD, and DD + R + γ models quantified via inverse modelling using Cl^- as a tracer in column 2. The ± symbol denote the parameter's standard errors.

	ADE	DD	DD + R + γ
R^2 (−)	0.845	0.771	0.989
MSE ((mg/l)^2)	936.9	1550	77.65
v (cm/min)	0.21 ± 0.02	0.24 ± 0.03	0.30 ± 0.33
D (cm^2)	0.994 ± 0.10	0.374 ± 0.73	0.496 ± 0.62
θ_{im} (−)	–	0.285 ± 0.26	0.253 ± 0.06
R (−)	–	–	1.90 ± 0.22
α (1/min)	–	0.015 ± 0.016	0.014 ± 0.017
γ_l (mgcm^3/min)	–	–	0.90*
γ_s (mgcm^3/min)	–	–	2.0*

* γ_l and γ_s were adjusted manually.

solid) governing the solute dynamics. On this pursuit, γ_l is nearly half of γ_s, suggesting a greater solute availability in the solid phase compared to the liquid phase. This may reflect the presence of the halophytic plant residuals embedded within the soil matrix, which can act as a persistent Cl^- source (Volik et al., 2018).

3.3. Sequential extraction results for selected TE

The comparison of sequential extraction results for pre and post experiment (Fig. 6) revealed minimal changes in the distribution of TE across the major geochemical fractions. However, two significant variations emerged: i) an increase in TE concentrations in the post experiment extraction, specifically in the crystalline Fe(III)-oxides fraction, and ii) a decrease in both As and Fe concentrations in the Fe(II)-sulphides fraction after the experiment.

4. Discussion

Usually, the reduced dissolution of Fe-(oxy)hydroxides and the anoxic SOM mineralization are the major drivers of As release in groundwater (Schiavo et al., 2024). In this study, because the ORP never became negative, the As increase in the leachate was likely attributable to FeAsS (or arsenian pyrite) oxidation, coupled with the desorption of As previously adsorbed onto the pyrite surface in the peat-bearing deposit (Amorosi and Sammartino, 2024). Moreover, As is known to be structurally incorporated in FeS_2 pyrite at significant proportions (up to 10 % wt) (Blanchard et al., 2007), and pyrite with As impurities oxidizes even faster than pyrite with very low impurity concentration (Lehner and Savage, 2008). Indeed, SOM-rich, sulphur-bearing lowland environments can function as effective geochemical traps for As under reducing conditions (Stuckey et al., 2015). Moreover, the chemical composition of the leaching water in the last stages of the experiments is an indirect proof that pyrite is ubiquitously present in SOM rich Holocene sediments constituting the aquifer/aquitard continuum in the Po deltaic area (Amorosi et al., 2002; Di Giuseppe et al., 2014) and could be oxidized at different stages during flushing with oxic waters. Despite this, no corresponding increase in dissolved Fe was detected, likely due to its precipitation as crystalline Fe(III)-oxides such as goethite and hematite. Indeed, the decrease in both As and Fe concentrations in the Fe (II)-sulphides fraction detected in the sequential extraction is consistent with the mobilization of As and Fe during the column experiment as a result of pyrite and FeAsS (or arsenian pyrite) oxidation. On the other hand, the observed increase in the fraction of crystalline Fe(III)-oxides can be explained by secondary precipitation processes (Heron et al., 1994). Particularly, Fe released during pyrite oxidation underwent hydrolysis, subsequently forming more crystalline Fe(III)-oxides (Guimarães et al., 2007; Zhao et al., 2024). This mineralogical transformation acted as a sink for Fe and the other TE, favouring their incorporation into the newly formed crystalline Fe(III)-oxides, highlighting their role as effective scavengers for TE under oxidizing conditions (Frierdich et al., 2011).

The following concentration increase of major and TEs after each flow interruption was probably due to the combination between the formation of anoxic microsites and the intra-particle diffusion. Indeed, in peaty environments, the fast organic matter degradation can lead to the formation of reducing micro-zones even in the presence of high ORP at column scale (Lacroix et al., 2023). In such anoxic microsites, the dissolution of Fe-oxides can act as a temporary source of TEs (Wehrer et al., 2017) that continued to diffuse within the soil matrix during the interruption period, following the intra-particle concentration gradients, followed by back-diffusion into the mobile zone when the flow restarts (Carstens et al., 2017). It should be stressed that the peaks observed immediately after the flow interruption phases are not merely artefacts of the column setup but rather reflect the dynamic geochemical processes that may also occur under field conditions and are evidence of the availability of these TE in the Po Delta aquitards/aquifers system (Habakaramo Macumu et al., 2024). In real-world scenarios, such as agricultural systems with intermittent irrigation or aquifer restoration strategies, flow interruptions are common (Addab and Bailey, 2022; El-Ghannam et al., 2021). These transient phases can promote the leaching of undesirable TE, as shown in this study. Therefore, the observed responses to the flow interruptions underscore the importance of accounting for this behaviour when designing and managing field-scale remediation or groundwater management interventions.

Regarding the experiment with the NaCl tracer test, the slightly augmented ionic strength of the flushing water carried into solution several major and TE. Tan et al. (2022) observed a similar pattern of TE leaching in a column experiment simulating the freshwater-seawater interface, characterized by distinct peaks in TE concentration during the seawater elution phase. This phenomenon was attributed to the competitive exchange between Na^+ and the TE strongly adsorbed onto colloidal surfaces, resulting in an enhanced mobilization of TE in the solution. Indeed, as proof of this mechanism, the observed Na^+ concentration after the peak was almost one quarter less than the corresponding Cl^- converted in meq/l, indicating active ion exchange. This behaviour poses a further challenge for aquifer remediation via freshwater flushing, particularly in regions where salt accumulation in the vadose zone through evapoconcentration processes may promote the downward migration of solute-enriched water (Li et al., 2014). In addition, the cross comparison between the pre-experiment exchangeable fraction and the column 2 cumulative leaching (Table 4) demonstrated that the combination of flow interruption and the NaCl tracer flushing led to a greater TE mobilization exceeding the concentrations observed in the exchangeable fraction for As, Fe, Ni and Pb, thus sourcing them from less available pools like amorphous and mineral

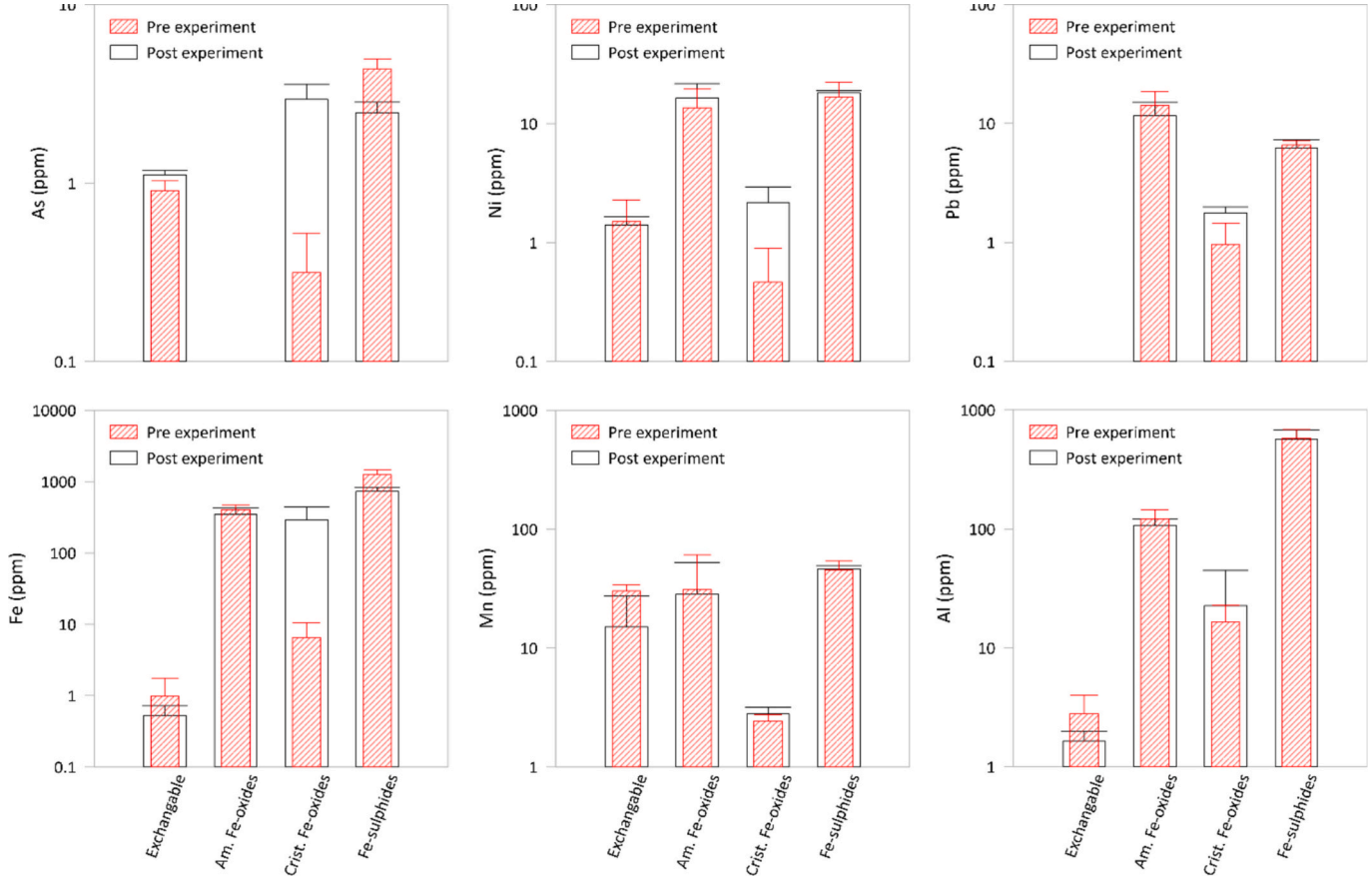

Fig. 6. Sequential extraction of selected TE, pre and post column experiments. Error bars denote standard deviations calculated on three replicas.

Table 4
Cross-comparison among the exchangeable fraction from the sequential extraction (pre-experiment) and the cumulative leaching from column 2 for selected TE.

Parameter (ppm)	Al	As	Fe	Mn	Ni	Pb
Cumulative leaching from rainwater	2.24	0.31	2.74	7.28	0.08	0.03
Cumulative leaching from NaCl	0.34	0.02	0.15	0.38	0.08	0.03
Total cumulative leaching	2.58	0.33	2.89	7.66	0.16	0.06
Exch. fraction from TE	1.14	–	0.47	15.2	0.09	–

phases; while Mn was entirely attributable to the exchangeable pool. However, it is important to note that in field conditions, irrigation alternating with periods of no irrigation, along with the leaching of evapoconcentrated salts, could further exacerbate the mobilization of TE.

5. Conclusions

Column experiments were conducted on a salinized peaty soil from the Po Delta. Results indicate that periodic irrigation can potentially leach salts into the shallow groundwater or into the surface waters via tile drains. The initial concentrations of TE exceeded the acceptable WHO threshold for domestic use, but after elution beyond 20 pore volumes, concentrations fell below the permissible levels, confirming the leaching of TE towards groundwater and/or surface water, raising concerns about potential water pollution. During periodic flow interruptions, the concentrations of TE rose again above the permissible WHO threshold, implying that the first irrigation events may be marked by the elution of elevated TE concentrations due to back diffusion from the immobile porosity fraction. Similarly, the dosage of NaCl to replicate evapoconcentrated solutes flushed from the topsoil was characterized by significant TE releases due to Na^+ cation exchanges with other major ions and TE. Additionally, relatively high concentrations of TE were observed in samples with abundant SOM fragments, which aligns with the findings of Habakaramo Macumu et al. (2024), alongside symptoms of pyrite and FeAsS (or arsenian pyrite) oxidation, leading to significant TE releases in the crystalline Fe(III)-oxides. The model results highlighted the critical influence of mobile-immobile porosity and desorption from SOM on solute transport, emphasizing the role of the halophytic SOM residues as a persistent source of additional salinity and TE. To the best of the authors' knowledge, this is the first study to couple flow interruptions with saline water flushing to simulate the enhanced TE release due to alternating sub-irrigation and evapoconcentration processes. The findings of this study are of particular relevance as similar hydrogeological settings are widespread globally. In light of these results, there is a compelling need for future research aimed at improving the understanding of the release of TE into shallow aquifers and aquitards characterized by elevated SOM and peaty layers.

CRediT authorship contribution statement

Abraham Ofori: Writing – original draft, Methodology, Investigation, Formal analysis, Data curation. **Luigi Alessandrino:** Writing – review & editing, Validation, Software, Methodology. **Regmi Vipin:** Investigation, Formal analysis, Data curation. **Micòl Mastrocicco:** Writing – review & editing, Validation, Supervision, Resources, Methodology. **Nicolò Colombani:** Writing – original draft, Visualization, Software, Resources, Methodology, Funding acquisition, Conceptualization.

Declaration of competing interest

The authors declare that they have no known competing financial interests or personal relationships that could have appeared to influence the work reported in this paper.

Acknowledgements

We acknowledge financial support under the National Recovery and Resilience Plan (NRRP), Mission 4, Component 2, Investment 1.1, Call for tender No. 104 published on 2.2.2022 by the Italian Ministry of University and Research (MUR), funded by the European Union – NextGenerationEU, Project Title NO3EXCESS - Nitrogen Origin, EXport and Cycling in coastal irrigatEd SettingS – CUP F53D23002160001 - Grant Assignment Decree No. 2022AKA3HL adopted on 30/06/2024 by the Italian Ministry of University and Research (MUR).

Data availability

Data will be made available on request.

References

Acosta, J.A., Jansen, B., Kalbitz, K., Faz, A., Martínez-Martínez, S., 2011. Salinity increases mobility of heavy metals in soils. Chemosphere 85 (8), 1318–1324. https://doi.org/10.1016/j.chemosphere.2011.07.046.

Addab, H., Bailey, R.T., 2022. Simulating the effect of subsurface tile drainage on watershed salinity using SWAT. Agric Water Manag 262, 107431. https://doi.org/10.1016/j.agwat.2021.107431.

Alessandrino, L., Colombani, N., Aschonitis, V., Eusebi, A.L., Mastrocicco, M., 2023. Performance of graphene and traditional soil improvers in limiting nutrients and heavy metals leaching from a sandy Calcisol. Sci. Total Environ. 858, 159806. https://doi.org/10.1016/j.scitotenv.2022.159806.

Amorosi, A., Sammartino, I., 2024. Predicting natural arsenic enrichment in peat-bearing, alluvial and coastal depositional systems: a generalized model based on sequence stratigraphy. Sci. Total Environ. 924, 171571. https://doi.org/10.1016/j.scitotenv.2024.171571.

Amorosi, A., Centineo, M.C., Dinelli, E., Lucchini, F., Tateo, F., 2002. Geochemical and mineralogical variations as indicators of provenance changes in Late Quaternary deposits of SE Po Plain. Sediment. Geol. 151 (3–4), 273–292. https://doi.org/10.1016/s0037-0738(01)00261-5.

Appelo, C.A.J., Verweij, E., Schäfer, H., 1998. A hydrogeochemical transport model for an oxidation experiment with pyrite/calcite/exchangers/organic matter containing sand. Appl. Geochem. 13 (2), 257–268. https://doi.org/10.1016/S0883-2927(97)00070-X.

Bäckström, M., Karlsson, S., Bäckman, L., Folkeson, L., Lind, B., 2004. Mobilisation of heavy metals by deicing salts in a roadside environment. Water Res. 38 (3), 720–732. https://doi.org/10.1016/j.watres.2003.11.006.

Bacon, J.R., Davidson, C.M., 2008. Is there a future for sequential chemical extraction? Analyst 133 (1), 25–46. https://doi.org/10.1039/B711896A.

Bakircioglu, D., Kurtulus, Y.B., Yurtsever, S., 2013. Comparison of extraction induced by emulsion breaking, ultrasonic extraction, and wet digestion procedures for determination of metals in edible oil samples in Turkey using ICP-OES. Food Chem. 138 (2–3), 770–775. https://doi.org/10.1016/j.foodchem.2012.10.089.

Bao, Y., Bolan, N.S., Lai, J., Wang, Y., Jin, X., Kirkham, M.B., Wu, X., Fang, Z., Zhang, Y., Wang, H., 2022. Interactions between organic matter and Fe (hydr) oxides and their influences on immobilization and remobilization of metal (loid) s: a review. Crit. Rev. Environ. Sci. Technol. 52 (22), 4016–4037. https://doi.org/10.1080/10643389.2021.1974766.

Bianchini, G., Natali, C., Di Giuseppe, D., Beccaluva, L., 2012. Heavy metals in soils and sedimentary deposits of the Padanian Plain (Ferrara, Northern Italy): characterisation and biomonitoring. J. Soil Sediment. 12 (7), 1145–1153. https://doi.org/10.1007/s11368-012-0538-5.

Blanchard, M., Alfredsson, M., Brodholt, J., Wright, K., Catlow, C.R.A., 2007. Arsenic incorporation into FeS_2 pyrite and its influence on dissolution: a DFT study. Geochim. Cosmochim. Acta 71, 624–630. https://doi.org/10.1016/j.gca.2006.09.021.

Botter, G., Peratoner, F., Putti, M., Zuliani, A., Zonta, R., Rinaldo, A., Marani, M., 2008. Observation and modeling of catchment-scale solute transport in the hydrologic response: a tracer study. Water Resour. Res. 44 (5). https://doi.org/10.1029/2007WR006611.

Caporale, A.G., Violante, A., 2016. Chemical processes affecting the mobility of heavy metals and metalloids in soil environments. Curr. Pollut. Rep. 2, 15–27. https://doi.org/10.1007/s40726-015-0024-y.

Capuano, R.M., Jones, C.R., 2020. Cation exchange in groundwater-chemical evolution and prediction of paleo-groundwater flow: a natural-system study. Water Resour. Res. 56 (8), e2019WR026318. https://doi.org/10.1029/2019WR026318.

Carrillo-González, R., Šimůnek, J., Sauvé, S., Adriano, D., 2006. Mechanisms and pathways of trace element mobility in soils. Adv. Agron. 91, 111–178. https://doi.org/10.1016/S0065-2113(06)91003-7.

Carstens, J.F., Bachmann, J., Neuweiler, I., 2017. Effects of flow interruption on transport and retention of iron oxide colloids in quartz sand. Colloids Surf. A Physicochem. Eng. Asp. 520, 532–543. https://doi.org/10.1016/j.colsurfa.2017.02.003.

Chakraborty, P., Chakrabarti, C.L., 2006. Chemical speciation of Co, Ni, Cu, and Zn in mine effluents and effects of dilution of the effluent on release of the above metals from their metal–dissolved organic carbon (DOC) complexes. Anal. Chim. Acta 571 (2), 260–269. https://doi.org/10.1016/j.aca.2006.04.069.

Chandra, A.P., Gerson, A.R., 2010. The mechanisms of pyrite oxidation and leaching: a fundamental perspective. Surf. Sci. Rep. 65 (9), 293–315. https://doi.org/10.1016/j.surfrep.2010.08.003.

Colombani, N., Gervasio, M.P., Castaldelli, G., Mastrocicco, M., 2020. Soil conditioners effects on hydraulic properties, leaching processes and denitrification on a silty-clay soil. Sci. Total Environ. 733, 139342. https://doi.org/10.1016/j.scitotenv.2020.139342.

Cook, S., Peacock, M., Evans, C.D., Page, S.E., Whelan, M.J., Gauci, V., Kho, L.K., 2017. Quantifying tropical peatland dissolved organic carbon (DOC) using UV-visible spectroscopy. Water Res. 115, 229–235. https://doi.org/10.1016/j.watres.2017.02.059.

Corkhill, C.L., Vaughan, D.J., 2009. Arsenopyrite oxidation–a review. Appl. Geochem. 24 (12), 2342–2361. https://doi.org/10.1016/j.apgeochem.2009.09.008.

Dahmouni, M., Hoermann, G., Jouzdan, O., Hachicha, M., 2018. Export of salt and heavy metals in an area irrigated with treated wastewater: a case study from Cebala Borj-Touil (Tunisia). Desalin. Water Treat. 102, 61–70. https://doi.org/10.5004/dwt.2018.21825.

D'Archivio, A.A., Foschi, M., Aloia, R., Maggi, M.A., Rossi, L., Ruggieri, F., 2019. Geographical discrimination of red garlic (Allium sativum L.) produced in Italy by means of multivariate statistical analysis of ICP-OES data. Food Chem. 275, 333–338. https://doi.org/10.1016/j.foodchem.2018.09.088.

Davidson, C.M., Thomas, R.P., McVey, S.E., Perala, R., Littlejohn, D., Ure, A.M., 1994. Evaluation of a sequential extraction procedure for the speciation of heavy metals in sediments. Anal. Chim. Acta 291 (3), 277–286. https://doi.org/10.1016/0003-2670(94)80023-5.

de Andrade Passos, E., Alves, J.C., dos Santos, I.S., Alves, J.D.P.H., Garcia, C.A.B., Costa, A.C.S., 2010. Assessment of trace metals contamination in estuarine sediments using a sequential extraction technique and principal component analysis. Microchem. J. 96 (1), 50–57. https://doi.org/10.1016/j.microc.2010.01.018.

Di Giuseppe, D., Faccini, B., Mastrocicco, M., Colombani, N., Coltorti, M., 2014. Reclamation influence and background geochemistry of neutral saline soils in the Po River Delta Plain (Northern Italy). Environ. Earth Sci. 72, 2457–2473. https://doi.org/10.1007/s12665-014-3154-4.

Dickson, A.G., 1981. An exact definition of total alkalinity and a procedure for the estimation of alkalinity and total inorganic carbon from titration data. Deep Sea Res Part A 28 (6), 609–623. https://doi.org/10.1016/0198-0149(81)90121-7.

Ding, W.W., Sturgeon, R.E., 1997. Minimization of transition metal interferences with hydride generation techniques. Anal. Chem. 69 (3), 527–531. https://doi.org/10.1021/ac9608026.

Douvris, C., Vaughan, T., Bussan, D., Bartzas, G., Thomas, R., 2023. How ICP-OES changed the face of trace element analysis: review of the global application landscape. Sci. Total Environ. 905, 167242. https://doi.org/10.1016/j.scitotenv.2023.167242.

Du Laing, G., Rinklebe, J., Vandecasteele, B., Meers, E., Tack, F.M., 2009. Trace metal behaviour in estuarine and riverine floodplain soils and sediments: a review. Sci. Total Environ. 407 (13), 3972–3985. https://doi.org/10.1016/j.scitotenv.2008.07.025.

Eeman, S., de Louw, P.G., Van der Zee, S.E.A.T.M., 2017. Cation exchange in a temporally fluctuating thin freshwater lens on top of saline groundwater. Hydrgeol. J. 25 (1), 223–241. https://doi.org/10.1007/s10040-016-1475-y.

El-Ghannam, M.K., Aiad, M.A., Abdallah, A.M., 2021. Irrigation efficiency, drain outflow and yield responses to drain depth in the Nile delta clay soil, Egypt. Agric. Water Manag. 246, 106674. https://doi.org/10.1016/j.agwat.2020.106674.

Fan, R., Qian, G., Li, Y., Short, M.D., Schumann, R.C., Chen, M., Smart, R.St.C., Gerson, A.R., 2022. Evolution of pyrite oxidation from a 10-year kinetic leach study: implications for secondary mineralisation in acid mine drainage control. Chem. Geol. 588, 120653. https://doi.org/10.1016/j.chemgeo.2021.120653.

Farooq, S.H., Chandrasekharam, D., Berner, Z., Norra, S., Stüben, D., 2010. Influence of traditional agricultural practices on mobilization of arsenic from sediments to groundwater in Bengal delta. Water Res. 44 (19), 5575–5588. https://doi.org/10.1016/j.watres.2010.05.057.

Feinstein, D.T., Guo, W., 2004. STANMOD: a suite of windows-based programs for evaluating solute transport. Ground Water 42 (4), 482. https://doi.org/10.1111/j.1745-6584.2004.tb02615.x.

Fontes, M.P.F., dos Santos, G.C., 2010. Lability and sorption of heavy metals as related to chemical, physical, and mineralogical characteristics of highly weathered soils. J. Soils Sediments 10, 774–786. https://doi.org/10.1007/s11368-009-0157-y.

Freeman, C., Ostle, N., Kang, H., 2001. An enzymic 'latch' on a global carbon store: a shortage of oxygen locks up carbon in peatlands by restraining a single enzymes. Nature 409 (6817), 149. https://doi.org/10.1038/35051650.

Frierdich, A.J., Luo, Y., Catalano, J.G., 2011. Trace element cycling through iron oxide minerals during redox-driven dynamic recrystallization. Geology 39 (11), 1083–1086. https://doi.org/10.1130/g32330.1.

Frohne, T., Rinklebe, J., Diaz-Bone, R.A., Du Laing, G., 2011. Controlled variation of redox conditions in a floodplain soil: impact on metal mobilization and

biomethylation of arsenic and antimony. Geoderma 160 (3–4), 414–424. https://doi.org/10.1016/j.geoderma.2010.10.012.
Gaiolini, M., Colombani, N., Chierici, V., Montanari, L., Mastrocicco, M., 2025. Numerical modelling of groundwater level and salinity evolution in a low-lying coastal area under intensive agricultural activity. Water Resour. Manag. 39 (4), 1747–1761. https://doi.org/10.1007/s11269-024-04044-y.
Gantayat, R.R., Elumalai, V., 2024. Salinity-induced changes in heavy metal behavior and mobility in semi-arid coastal aquifers: a comprehensive review. Water 16 (7), 1052. https://doi.org/10.3390/w16071052.
Giambastiani, B.M.S., Greggio, N., Carloni, G., Molducci, M., Antonellini, M., 2024. Potentially toxic elements (PTEs) distribution in drainage canal sediments of a low-lying coastal area. Earth Space Sci. 11, e2023EA003145. https://doi.org/10.1029/2023EA003145.
Gómez-Ariza, J.L., Giráldez, I., Sánchez-Rodas, D., Morales, E., 1999. Optimization of a sequential extraction scheme for the characterization of heavy metal mobility in iron oxide rich sediments. Int. J. Environ. Anal. Chem. 75 (1–2), 3–18. https://doi.org/10.1080/03067319908047296.
Gorham, E., 1991. Northern peatlands: role in the carbon cycle and probable responses to climatic warming. Ecol. Appl. 1 (2), 182–195. https://doi.org/10.2307/1941811.
Gu, J., Salem, A., Chen, Z., 2013. Lagoons of the Nile delta, Egypt, heavy metal sink: with a special reference to the Yangtze estuary of China. Estuar. Coast. Shelf Sci. 117, 282–292. https://doi.org/10.1016/j.ecss.2012.06.012.
Guimarães, L., de Abreu, H.A., Duarte, H.A., 2007. Fe(II) hydrolysis in aqueous solution: a DFT study. Chem. Phys. 333 (1), 10–17. https://doi.org/10.1016/j.chemphys.2006.12.023.
Habakaramo Macumu, P., Gaiolini, M., Ofori, A., Mastrocicco, M., Colombani, N., 2024. Additional sources of salinity and heavy metals from plant residues of peaty horizons in the Po River lowland (Italy). Sci. Total Environ. 957 (20), 177671. https://doi.org/10.1016/j.scitotenv.2024.177671.
Heron, G., Crouzet, C., Bourg, A.C.M., Christensen, T.H., 1994. Speciation of Fe(II) and Fe(III) in contaminated aquifer sediments using chemical extraction techniques. Environ. Sci. Tech. 28 (9), 1698–1705. https://doi.org/10.1021/es00058a023.
Höll, B.S., Fiedler, S., Jungkunst, H.F., Kalbitz, K., Freibauer, A., Drösler, M., Stahr, K., 2009. Characteristics of dissolved organic matter following 20 years of peatland restoration. Sci. Total Environ. 408 (1), 78–83. https://doi.org/10.1016/j.scitotenv.2009.08.046.
Huang, W.J., Wang, Y., Cai, W.J., 2012. Assessment of sample storage techniques for total alkalinity and dissolved inorganic carbon in seawater. Limnol. Oceanogr. Methods 10 (9), 711–717. https://doi.org/10.4319/lom.2012.10.711.
Husson, O., 2013. Redox potential (Eh) and pH as drivers of soil/plant/microorganism systems: a transdisciplinary overview pointing to integrative opportunities for agronomy. Plant and Soil 362, 389–417. https://doi.org/10.1007/s11104-012-1429-7.
Jacques, D., Šimůnek, J., Mallants, D., Van Genuchten, M.T., 2008. Modelling coupled water flow, solute transport and geochemical reactions affecting heavy metal migration in a podzol soil. Geoderma 145 (3–4), 449–461. https://doi.org/10.1016/j.geoderma.2008.01.00.
Kelepertzis, E., Stathopoulou, E., 2013. Availability of geogenic heavy metals in soils of Thiva town (central Greece). Environ. Monit. Assess. 185 (11), 9603–9618. https://doi.org/10.1007/s10661-013-3277-1.
Keon, N.E., Swartz, C.H., Brabander, D.J., Harvey, C., Hemond, H.F., 2001. Validation of an arsenic sequential extraction method for evaluating mobility in sediments. Environ. Sci. Technol. 35 (13), 2778–2784. https://doi.org/10.1021/es001511o.
Khan, S.R., Sharma, B., Chawla, P.A., Bhatia, R., 2022. Inductively coupled plasma optical emission spectrometry (ICP-OES): a powerful analytical technique for elemental analysis. Food Anal. Methods 15 (3), 666–688. https://doi.org/10.1007/s12161-021-02148-4.
Kiecak, A., Breuer, F., Stumpp, C., 2019. Column experiments on sorption coefficients and biodegradation rates of selected pharmaceuticals in three aquifer sediments. Water 12 (1), 14. https://doi.org/10.3390/w12010014.
Kim, J., Hyun, S., 2015. Nonequilibrium leaching behavior of metallic elements (Cu, Zn, As, Cd, and Pb) from soils collected from long-term abandoned mine sites. Chemosphere 134, 150–158. https://doi.org/10.1016/j.chemosphere.2015.04.018.
Kryc, K.A., Murray, R.W., Murray, D.W., 2003. Elemental fractionation of Si, Al, Ti, Fe, Ca, Mn, P, and Ba in five marine sedimentary reference materials: results from sequential extractions. Anal. Chim. Acta 487 (1), 117–128. https://doi.org/10.1016/S0003-2670(03)00492-6.
Lacroix, E.M., Aeppli, M., Boye, K., Brodie, E., Fendorf, S., Keiluweit, M., Naughton, H.R., Noël, V., Sihi, D., 2023. Consider the anoxic microsite: acknowledging and appreciating spatiotemporal redox heterogeneity in soils and sediments. ACS Earth Space Chem. 7 (9), 1592–1609. https://doi.org/10.1021/acsearthspacechem.3c00032.
Lehner, S., Savage, K., 2008. The effect of As, Co, and Ni impurities on pyrite oxidation kinetics: batch and flow-through reactor experiments with synthetic pyrite. Geochim. Cosmochim. Acta 72, 1788–1800. https://doi.org/10.1016/j.gca.2008.02.003.
Lengke, M.F., Sanpawanitchakit, C., Tempel, R.N., 2009. The oxidation and dissolution of arsenic-bearing sulfides. Can. Mineral. 47 (3), 593–613. https://doi.org/10.3749/canmin.47.3.593.
Lewis, J., Sjöstrom, J., 2010. Optimizing the experimental design of soil columns in saturated and unsaturated transport experiments. J. Contam. Hydrol. 115 (1–4), 1–13. https://doi.org/10.1016/j.jconhyd.2010.04.001.
Li, X., Chang, S.X., Salifu, K.F., 2014. Soil texture and layering effects on water and salt dynamics in the presence of a water table: a review. Environ. Rev. 22 (1), 41–50. https://doi.org/10.1139/er-2013-0035.
Li, H., Lu, J., Li, Q.S., He, B.Y., Mei, X.Q., Yu, D.P., Xu, Z.M., Guo, S.H., Chen, H.J., 2016. Effects of freshwater leaching on potential bioavailability of heavy metals in tidal flat soils. Environ. Geochem. Health 38, 99–110. https://doi.org/10.1007/s10653-015-9688-x.
Li, X., Wang, X., Yu, J., Yang, J., Yu, Y., Zhou, D., Li, Y., 2020. Effect of water level and salinity on metal fractionation in sediments of the Yellow River Delta. Wetlands 40, 2765–2774. https://doi.org/10.1007/s13157-020-01337-x.
Li, Y., Gao, B., Xu, D., Lu, J., Zhou, H., Gao, L., 2022a. Heavy metals in the water-level-fluctuation zone soil of the three Gorges Reservoir, China: remobilization and catchment-wide transportation. J. Hydrol. 612, 128108. https://doi.org/10.1016/j.jhydrol.2022.128108.
Li, Q., Wang, Y., Li, Y., Li, L., Tang, M., Hu, W., Chen, L., Ai, S., 2022b. Speciation of heavy metals in soils and their immobilization at micro-scale interfaces among diverse soil components. Sci. Total Environ. 825, 153862. https://doi.org/10.1016/j.scitotenv.2022.153862.
López Meza, S., Kalbe, U., Berger, W., Simon, F.G., 2010. Effect of contact time on the release of contaminants from granular waste materials during column leaching experiments. Waste Manag. 30 (4), 565–571. https://doi.org/10.1016/j.wasman.2009.11.022.
Ma, D., He, Z., Wang, L., Zhao, W., Chen, L., Lin, P., Zhao, P., Wang, W., Gao, Y., Li, J., 2023. Soil water and salt migration in oasis farmland during crop growing season. J. Soil. Sediment. 23 (1), 355–367. https://doi.org/10.1007/s11368-022-03322-9.
Mastrocicco, M., Prommer, H., Pasti, L., Palpacelli, S., Colombani, N., 2011. Evaluation of saline tracer performance during electrical conductivity groundwater monitoring. J. Contam. Hydrol. 123 (3–4), 157–166. https://doi.org/10.1016/j.jconhyd.2011.01.001.
McKibben, M.A., Barnes, H.L., 1986. Oxidation of pyrite in low temperature acidic solutions: rate laws and surface textures. Geochim. Cosmochim. Acta 50 (7), 1509–1520. https://doi.org/10.1016/0016-7037(86)90325-X.
Mensah, A.K., Amoakwah, E., 2024. Soil biogeochemical factors influencing mobilization of toxic. In: Perspectives and Insights on Soil Contamination and Effective Remediation Techniques, p. 41. https://doi.org/10.5772/intechopen.1005487.
Mora, A., Mahlknecht, J., Ledesma-Ruiz, R., Sanford, W.E., Lesser, L.E., 2020. Dynamics of major and trace elements during seawater intrusion in a coastal sedimentary aquifer impacted by anthropogenic activities. J. Contam. Hydrol. 232, 103653. https://doi.org/10.1016/j.jconhyd.2020.103653.
Nenova, L., Zgorelec, Z., Benkova, M., Semeomova, C., Velichkova, N., Atanassova, I., 2018. Solubility and availability of copper, zinc, lead, and iron in technosols under the effect of increasing copper levels. Int. J. Hydrol. 2, 379–386. https://doi.org/10.15406/ijh.2018.02.00100.
Pasternack, G.B., Brown, K.J., 2006. Natural and anthropogenic geochemical signatures of floodplain and deltaic sedimentary strata, Sacramento–San Joaquin Delta, California, USA. Environ. Pollut. 141 (2), 295–309. https://doi.org/10.1016/j.envpol.2005.08.044.
Pelfrêne, A., Gassama, N., Grimaud, D., 2009. Mobility of major-, minor-and trace elements in solutions of a planosolic soil: distribution and controlling factors. Appl. Geochem. 24 (1), 96–105. https://doi.org/10.1016/j.apgeochem.2008.11.00.
Pérez-Esteban, J., Escolástico, C., Moliner, A., Masaguer, A., 2013. Chemical speciation and mobilization of copper and zinc in naturally contaminated mine soils with citric and tartaric acids. Chemosphere 90 (2), 276–283. https://doi.org/10.1016/j.chemosphere.2012.06.065.
Pradhan, S.K., Ambade, B., 2020. Extractive separation of rare earth elements and their determination by inductively coupled plasma optical emission spectrometry in geological samples. J. Anal. At. Spectrom 35 (7), 1395–1404. https://doi.org/10.1039/D0JA00190B.
Qian, Y., Zhang, W., Yu, L., Feng, H., 2015. Metal pollution in coastal sediments. Curr. Pollut. Rep. 1, 203–219. https://doi.org/10.1007/s40726-015-0018-9.
Rahman, Z., Singh, V.P., 2019. The relative impact of toxic heavy metals (THMs)arsenic (As), cadmium (Cd), chromium (Cr)(VI), mercury (Hg), and lead (Pb) on the total environment: an overview. Environ. Monit. Assess. 191, 1–21. https://doi.org/10.1007/s10661-019-7528-7.
Rao, C.R.M., Sahuquillo, A., Lopez Sanchez, J.F., 2008. A review of the different methods applied in environmental geochemistry for single and sequential extraction of trace elements in soils and related materials. Water Air Soil Pollut. 189 (1), 291–333. https://doi.org/10.1007/s11270-007-9564-0.
Saaltink, M.W., Rodríguez-Escales, P., 2022. Modeling the organic carbon oxidation and redox sequence under the partial-equilibrium approach: a discussion by means of a semi-analytical solution. Water Resour. Res. 58 (7), e2021WR031194. https://doi.org/10.1029/2021WR031194.
Sahuquillo, A., Rigol, A., Rauret, G., 2003. Overview of the use of leaching/extraction tests for risk assessment of trace metals in contaminated soils and sediments. TrAC Trends Anal. Chem. 22 (3), 152–159. https://doi.org/10.1016/S0165-9936(03)00303-0.
Said, I., Salman, S.A., Elnazer, A.A., 2022. Salinization of groundwater during 20 years of agricultural irrigation, Luxor, Egypt. Environ. Geochem. Health 44, 3821–3835. https://doi.org/10.1007/s10653-021-01135-2.
Salomons, W., Förstner, U.J.E.T., 1980. Trace metal analysis on polluted sediments: part II: evaluation of environmental impact. Environ. Technol. 1 (11), 506–517. https://doi.org/10.1080/09593338009384007.
Santelli, C.M., Welch, S.A., Westrich, H.R., Banfield, J.F., 2001. The effect of Fe-oxidizing bacteria on Fe-silicate mineral dissolution. Chem. Geol. 180, 99–115. https://doi.org/10.1016/s0009-2541(01)00308-4.
Sarkar, S.K., Favas, P.J., Rakshit, D., Satpathy, K.K., Hernandez-Soriano, M.C., 2014. Geochemical speciation and risk assessment of heavy metals in soils and sediments. In: Environmental Risk Assessment of Soil Contamination. IntechOpen doi:https://doi.org/10.5772/5729.

Sbarbati, C., Barbieri, M., Barron, A., Bostick, B., Colombani, N., Mastrocicco, M., Prommer, H., Passaretti, S., Zheng, Y., Petitta, M., 2020. Redox dependent arsenic occurrence and partitioning in an industrial coastal aquifer: evidence from high spatial resolution characterization of groundwater and sediments. Water 12 (10), 2932. https://doi.org/10.3390/w12102932.

Schiavo, M., Giambastiani, B.M.S., Greggio, N., Colombani, N., Mastrocicco, M., 2024. Geostatistical assessment of groundwater arsenic contamination in the Padana Plain. Sci. Total Environ. 931, 172998. https://doi.org/10.1016/j.scitotenv.2024.172998.

Schulz-Zunkel, C., Krueger, F., 2009. Trace metal dynamics in floodplain soils of the River Elbe: a review. J. Environ. Qual. 38, 1349–1362. https://doi.org/10.2134/jeq2008.0299.

Seuntjens, P., Nowack, B., Schulin, R., 2004. Root-zone modeling of heavy metal uptake and leaching in the presence of organic ligands. Plant and Soil 265, 61–73. https://doi.org/10.1007/s11104-005-8470-8.

Shams, M., Tavakkoli Nezhad, N., Dehghan, A., Alidadi, H., Paydar, M., Mohammadi, A. A., Zarei, A., 2022. Heavy metals exposure, carcinogenic and non-carcinogenic human health risks assessment of groundwater around mines in Joghatai, Iran. Int. J. Environ. Anal. Chem. 102 (8), 1884–1899. https://doi.org/10.1080/03067319.2020.1743835.

Simeoni, U., Corbau, C., 2009. A review of the Delta Po evolution (Italy) related to climatic changes and human impacts. Geomorphology 107 (1–2), 64–71. https://doi.org/10.1016/j.geomorph.2008.11.004.

Sposito, G. (Ed.), 1995. The Environmental Chemistry of Aluminum, 2nd ed. CRC Press. https://doi.org/10.1201/9780138736781.

Standing Committee of Analysts, 2018. Bluebook 263. The Determination of Metals in Raw and Potable Waters by Inductively Coupled Plasma Optical Emission Spectrometry (ICP-OES). https://standingcommitteeofanalysts.co.uk/wp-content/uploads/Blue_Book_Library/263.pdf.

Stuckey, J.W., Schaefer, M.V., Kocar, B.D., Dittmar, J., Pacheco, J.L., Benner, S.G., Fendorf, S., 2015. Peat formation concentrates arsenic within sediment deposits of the Mekong Delta. Geochim. Cosmochim. Acta 149, 190–205. https://doi.org/10.1016/j.gca.2014.10.021.

Tack, F.M.G., Verloo, M.G., 1995. Chemical speciation and fractionation in soil and sediment heavy metal analysis: a review. Int. J. Environ. Anal. Chem. 59 (2–4), 225–238. https://doi.org/10.1080/03067319508041330.

Tan, B., Liu, C., Tan, X., You, X., Dai, C., Liu, S., Li, J., Li, N., 2022. Heavy metal transport driven by seawater-freshwater interface dynamics: the role of colloid mobilization and aquifer pore structure change. Water Res. 217, 118370. https://doi.org/10.1016/j.watres.2022.118370.

Tang, J., Sakanakura, H., Nakagawa, M., Takai, A., Katsumi, T., 2020. Prediction of column leaching behaviour based on batch leaching tests with different liquid to solid ratios. Jpn. Geotech. Soc. Spec. Publ. 8 (2), 31–36. https://doi.org/10.3208/jgssp.v08.j21.

Tessier, A.P.G.C., Campbell, P.G., Bisson, M.J.A.C., 1979. Sequential extraction procedure for the speciation of particulate trace metals. Anal. Chem. 51 (7), 844–851. https://doi.org/10.1021/ac50043a017.

Thangavel, S., Dash, K., Dhavile, S.M., Sahayam, A.C., 2015. Determination of traces of As, B, Bi, Ga, Ge, P, Pb, Sb, Se, Si, and Te in high-purity nickel using inductively coupled plasma-optical emission spectrometry (ICP-OES). Talanta 131, 505–509. https://doi.org/10.1016/j.talanta.2014.08.026.

Tiemeyer, B., Pfaffner, N., Frank, S., Kaiser, K., Fiedler, S., 2017. Pore water velocity and ionic strength effects on DOC release from peat-sand mixtures: results from laboratory and field experiments. Geoderma 296, 86–97. https://doi.org/10.1016/j.geoderma.2017.02.024.

Tisserand, D., Daval, D., Truche, L., Fernandez-Martinez, A., Sarret, G., Spadini, L., Némery, J., 2024. Recommendations and good practices for dissolved organic carbon (DOC) analyses at low concentrations. MethodsX 12, 102663. https://doi.org/10.1016/j.mex.2024.102663.

Toride, N., Leij, F.J., Van Genuchten, M.T., 1995. The CXTFIT Code for Estimating Transport Parameters From Laboratory or Field Tracer Experiments, Vol. 2. US Salinity Laboratory, Research Report No. 137, Riverside, CA, pp. 59–85.

Tran, Y.T., Bajracharya, K., Barry, D.A., 1998. Anomalous cadmium adsorption in flow interruption experiments. Geoderma 84 (1–3), 169–184. https://doi.org/10.1016/S0016-7061(97)00127-4.

U.S. Environmental Protection Agency, 1996. Method 1669. Sampling Ambient Water for Trace Metals at EPA Water Quality Criteria Levels. https://www.epa.gov/sites/default/files/2015-10/documents/method_1669_1996.pdf.

Van Genuchten, M.T., Šimunek, J., Leij, F.J., Toride, N., Šejna, M., 2012. STANMOD: model use, calibration, and validation. Trans. ASABE 55 (4), 1355–1366. https://doi.org/10.13031/2013.42247.

Vincent, A., Benoit, P., Pot, V., Madrigal, I., Delgado-Moreno, L., Labat, C., 2007. Impact of different land uses on the migration of two herbicides in a silt loam soil: unsaturated soil column displacement studies. Eur. J. Soil Sci. 58 (1), 320–328. https://doi.org/10.1111/j.1365-2389.2006.00844.x.

Vink, J.P., Harmsen, J., Rijnaarts, H., 2010. Delayed immobilization of heavy metals in soils and sediments under reducing and anaerobic conditions; consequences for flooding and storage. J. Soil. Sediment. 10, 1633–1645. https://doi.org/10.1007/s11368-010-0296-1.

Volik, O., Petrone, R.M., Wells, C.M., Price, J.S., 2018. Impact of salinity, hydrology and vegetation on long-term carbon accumulation in a saline boreal peatland and its implication for peatland reclamation in the Athabasca oil sands region. Wetlands 38 (2), 373–382. https://doi.org/10.1007/s13157-017-0974-5.

Wang, Y., Jiao, J.J., Zhang, K., Zhou, Y., 2016. Enrichment and mechanisms of heavy metal mobility in a coastal quaternary groundwater system of the Pearl River Delta, China. Sci. Total Environ. 545, 493–502. https://doi.org/10.1016/j.scitotenv.2015.12.01.

Wang, H., Dowd, P.A., Xu, C., 2019. A reaction rate model for pyrite oxidation considering the influence of water content and temperature. Miner. Eng. 134, 345–355. https://doi.org/10.1016/j.mineng.2019.02.002.

Wehrer, M., Totsche, K.U., 2008. Effective rates of heavy metal release from alkaline wastes—quantified by column outflow experiments and inverse simulations. J. Contam. Hydrol. 101 (1–4), 53–66. https://doi.org/10.1016/j.jconhyd.2008.07.005.

Wickstrøm, T., Lund, W., Bye, R., 1995. Determination of arsenic and tellurium by hydride generation atomic spectrometry: minimizing interferences from nickel, cobalt and copper by using an alkaline sample solution. Analyst 120 (11), 2695–2698. https://doi.org/10.1039/AN9952002695.

Wikiniyadhanee, R., Chotpantarat, S., Ong, S.K., 2015. Effects of kaolinite colloids on Cd^{2+} transport through saturated sand under varying ionic strength conditions: column experiments and modeling approaches. J. Contam. Hydrol. 182, 146–156. https://doi.org/10.1016/j.jconhyd.2015.08.008.

Wiltsche, H., Brenner, I.B., Prattes, K., Knapp, G., 2008. Characterization of a multimode sample introduction system (MSIS) for multielement analysis of trace elements in high alloy steels and nickel alloys using axially viewed hydride generation ICP-AES. J. Anal. At. Spectrom 23 (9), 1253–1262. https://doi.org/10.1039/b803943g.

Yousefi, S.R., Zolfonoun, E., 2020. A novel online hydride generation technique for the simultaneous determination of ultra trace amounts of hydride forming elements in water samples by inductively coupled plasma optical emission spectrometry. J. Anal. Chem. 75 (5), 595–599. https://doi.org/10.1134/S1061934820050196.

Zhang, Y., Weihermüller, L., Toth, B., Noman, M., Vereecken, H., 2022. Analyzing dual porosity in soil hydraulic properties using soil databases for pedotransfer function development. Vadose Zone J. 21 (5), e20227. https://doi.org/10.1002/vzj2.20227.

Zhao, Z., Chen, Y., Wu, D., 2024. Reactive oxidative species generation in pyrite abiotic-oxidation process: origins, influencing factors, applications for environmental remediation. Crit. Rev. Environ. Sci. Technol. 55 (6), 397–421. https://doi.org/10.1080/10643389.2024.2411793.